A Comparison of Teleseismic and Regional Seismic Moment Estimates in the European-Mediterranean Region

K. I. Konstantinou and S. Rontogianni
Institute of Geophysics, National Central University, Jhongli, Taiwan

INTRODUCTION

Since its first use by Aki (1966), seismic moment has been recognized as the most physically meaningful measure of the strength of the seismic source. The subsequent development of the moment magnitude scale further increased its usefulness, giving seismologists the opportunity to measure even the magnitude of very large events without concern about saturation effects. The routine computation of moment tensors and seismic moments has been made easier by the advent of efficient waveform inversion techniques. Dziewonski *et al.* (1981) pioneered the routine determination of moment tensors using teleseismic data for large events occurring worldwide. Their work led to the creation of the Global Centroid Moment Tensor (GCMT, formerly Harvard CMT) database, which contains thousands of moment tensor solutions and spans a period from early 1977 until present. Furthermore, the installation in the 1990s of many regional seismic networks equipped with broadband sensors made possible moment tensor inversions for smaller events that otherwise exhibited poor or even no teleseismic signal.

Many applications, such as regional seismic hazard evaluation or the calibration of relationships used for nuclear explosion discrimination (*e.g.*, Priestley and Patton 1997), critically depend on accurate estimates of seismic moment. In practice, however, several factors may lower the accuracy of these estimations. Patton (1998) showed that there are significant differences between GCMT and regional M_0 estimates in central Asia, where the teleseismic moments were larger by a factor of two to five for specific events. He suggested that such a bias may be caused by the thickness of the continental crust, which is not accounted for in the one-dimensional velocity model employed for teleseismic Green's functions calculations. Another proposed reason for the bias was data selection practices for smaller events that exhibit low signal-to-noise ratios. Subsequently, theoretical modeling indicated that incorrect model properties (such as crustal thickness) may introduce systematic amplitude variations to calculated Green's functions, leading to seismic moment discrepancies (Patton and Randall 2002).

More recently, Hjörleifsdottir and Ekström (2010) revisited this topic by investigating the influence of three-dimensional Earth structure on the GCMT moment tensor solutions. The authors calculated synthetic seismograms using global three-dimensional velocity models, simulating events that originate at different tectonic environments (mid-ocean ridges, subduction zones, continental collision areas). This dataset was later used as input to the GCMT inversion algorithm to check whether the method could accurately determine the source properties of the simulated events. The results showed a pattern of underestimation (10%–20%) of seismic moment in areas of crustal thinning such as the Mid-Atlantic Ridge and overestimation (15%–20%) in areas with thick crust such as central Asia. Overestimated (up to 54%) seismic moments were also found for events exhibiting low-angle thrust-faulting mechanisms associated with subduction zones. An important conclusion of these tests was that the inclusion of more than one wave type (body, surface waves) in the inversion can contribute toward a well-constrained seismic moment estimate.

The broader European-Mediterranean (EM) region encompasses seismically active areas (such as Greece, Italy, and Turkey) that are well monitored by a number of local and regional seismic networks. Currently, two groups routinely invert regional waveforms in order to derive moment tensor solutions for the EM region, namely the Regional Centroid Moment Tensor (RCMT) group (Pondrelli *et al.* 2002, 2004) and the Swiss Seismological Service (SED) group (Braunmiller *et al.* 2002). Both these databases contain manually determined solutions (*i.e.*, solutions reviewed for consistency by a human); however, since 2006 SED has implemented a fully automatic determination of moment tensors. It should be noted that the EM region is one of the very few places worldwide where a number of events may have multiple published moment tensor solutions. This study takes advantage of this fact in order to investigate the accuracy of seismic moment estimates derived using different algorithms/data and for earthquakes occurring across different tectonic regimes. In order to ensure that solutions are free of operational artifacts/errors, we consider only manual solutions. First, we give a brief description of the waveform inversion methodologies employed by the different groups. This is followed by comparison of teleseismic (GCMT) and regional (RCMT, SED) M_0 estimates through linear regression and the identification of events that exhibit large dis-

doi: 10.1785/gssrl.82.2.188

crepancies. Possible causes for these discrepancies are examined in conjunction with the results of the aforementioned studies. Hereafter, the term "residual" and the symbol $\Delta \log M_0$ will be used to refer to the difference of teleseismic minus regional seismic moment. Individual events will be mentioned in the text by their date (year, month, day; *e.g.*, 20030215).

MOMENT TENSOR INVERSION METHODOLOGIES

The GCMT algorithm inverts for the deviatoric moment tensor as well as the centroid location and time of each event by minimizing the difference between observed and synthetic waveforms. Unlike other inversion methods, this minimization is done in three different frequency bands and time windows corresponding to body (40–150 s), mantle (125–350 s), and surface waves (passband depends on event size). The inversion is set up in two steps, first fixing the location to the one reported by the Preliminary Determination of Epicenters (PDE) bulletin and inverting for the moment tensor and then also inverting for the centroid location and time of the event. For body and mantle waves, synthetic seismograms are calculated using normal-mode summation for the one-dimensional Earth model PREM (Dziewonski and Anderson 1981), while a correction for three-dimensional structure is made by applying path-averaged perturbations to the eigenfrequencies of the normal modes (Dziewonski *et al.* 1992). Surface-wave synthetics are calculated for the fundamental mode and overtones separately, with excitation and receiver terms computed using PREM.

The RCMT algorithm is an extension of the GCMT described above, and it is used for calculating centroid moment tensors for moderate-sized earthquakes utilizing regional waveforms (Arvidsson and Ekström 1998). This modified CMT method uses the first arriving surface waves with a lowpass cutoff period of 40–60 s. Even though these waves are well-excited by smaller events, they had not been previously included in the standard GCMT analysis since they are highly sensitive to lithospheric heterogeneities. However, accurate global phase velocity maps derived by Ekström *et al.* (1997) made possible the calculation of propagation dispersion characteristics of these waves, which is used for correcting the computed synthetic seismograms for the fundamental modes. The initial location of each event is again taken from the PDE reports and the inversion process follows the two steps outlined for the GCMT algorithm. In a similar fashion with GCMT, the PREM model is used for the calculation of source and receiver excitation functions.

On the other hand, the Swiss Seismological Service group uses a linear time-domain inversion proposed by Nabelek and Xia (1995) that minimizes the least-squares misfit between observed and synthetic waveforms. Originally the method could invert for both the moment tensor and source time of each event; however, the SED implementation fixes the time history to one triangular element. Complete three-component seismograms consisting of body and surface waves are used, and the inversion derives only the deviatoric part of the moment tensor. The best-fitting depth is found by a grid search over several trial depths every 3–4 km intervals. The passband utilized ranges from 10–30 s for small events occurring in Switzerland/central Europe, where station coverage is optimal, to a cutoff period of 40 s for more distant events. Synthetic seismograms are calculated using a four-layer over half-space velocity model suitable for the European-Mediterranean area (see Braunmiller *et al.* 2002). For events that occur in the Mid-Atlantic Ridge or the Middle East regions, PREM is used instead. Figure 1 graphically summarizes the three methodologies showing the wave types and passbands used.

GCMT VERSUS RCMT SEISMIC MOMENTS

The RCMT catalog covers the period 1997–2004 for the finally revised solutions, and 122 of them have also a corresponding

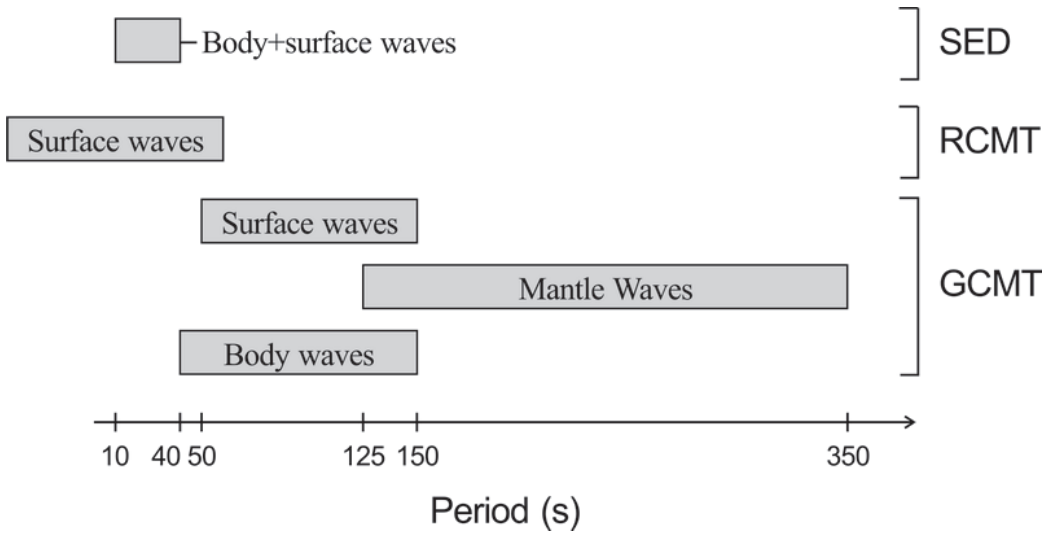

▲ **Figure 1.** Schematic illustration of the different wave types and passbands utilized by the GCMT, RCMT, and SED groups when performing moment tensor inversion (see text for more details).

GCMT solution. A direct comparison of the two estimates reveals that for the majority of the events there is almost no difference and the linear correlation is high (Figure 2). However, some events clearly have much larger teleseismic moments resulting in a least-squares fit that exhibits an underestimation trend for the regional M_0 estimates. The distribution of the logarithm of this difference (GCMT-RCMT) also confirms that. This underestimation trend had been also observed by Arvidsson and Ekström (1998) for the set of events they used as inversion examples when introducing the RCMT method. It is found that 24 events (~20% of all events) have $\Delta\log M_0 > 0.20$, which essentially means seismic moment differences of more than 1.5 times, while one event shows a moment difference of 0.85 units (GCMT M_0 up to seven times larger than RCMT). Figure 3 shows the geographical distribution of the events. It can be seen that there is no clustering at any specific region, even though the largest residuals are observed in the eastern Mediterranean. Source parameters and other available information about these events is summarized in Table 1. The majority appear to have a shallow origin (<20 km) with many centroid depths fixed at 15 km, which is the shallowest depth possible for stable CMT inversions.

In order to investigate the causes of these M_0 differences, we examined a number of factors that could influence M_0 estimation. First, the seismic moment residuals are compared to body wave magnitudes (*mb*), crustal thickness at the source region of each event, and the similarity between GCMT and RCMT focal mechanisms through the use of the Kagan angle (Kagan 1991) (Figure 4). Patton (1998) found that large seismic moment residuals and body wave magnitudes for earthquakes in central Asia exhibited an inverse relationship, where larger residuals correlated with smaller *mb* values. Indeed, except in one event, all have body wave magnitudes smaller than 5.0; however, there does not seem to be any significant linear correlation between the two quantities. Crustal thickness at the source region of each event has been obtained from the global crustal model CRUST2.0 (Bassin *et al.* 2000). Again, only one event has occurred in a region where the crust is significantly thicker (~43 km) than the thickness assumed in PREM, and it is also the event that exhibits the largest residual. On the other hand, nine events have Kagan angles smaller than 25°, implying that focal mechanism consistency between GCMT and RCMT does not necessarily reflect consistency in seismic moment estimation (actually the two events with the largest residuals exhibit relatively small Kagan angles).

Similar to the study of Patton (1998), the small magnitude of most events points to the possibility that the number of stations used in each CMT inversion may have an effect on moment residuals. For the RCMT catalog the number of stations included in the inversions of each event listed in Table 1 was usually more than 15, while for GCMT this number varied greatly. Figure 5 shows the temporal distribution of the 24 events as a function of the number of stations used in the GCMT inversion and the amplitude of the M_0 residual. It can be seen that the largest residuals coincide with a small number of stations, a trend that is becoming less pronounced

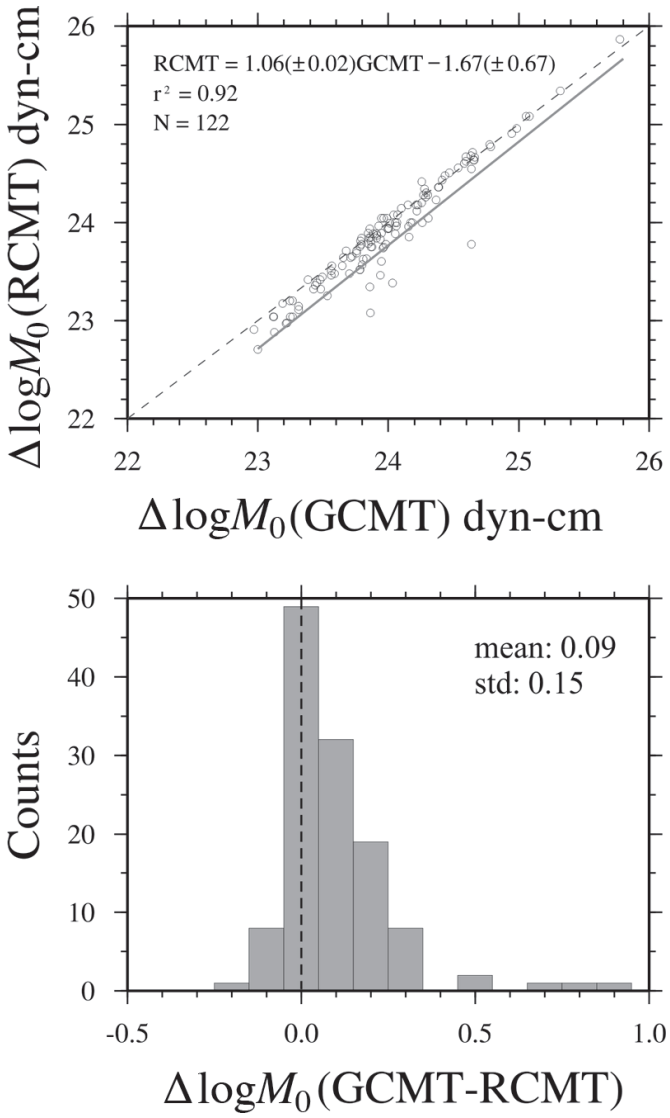

▲ **Figure 2.** Top panel: Linear regression results between RCMT and GCMT seismic moment estimates. The dashed line represents the 1:1 slope and the solid one the result of least-squares regression. *N* is the total number of events used and r^2 is the correlation coefficient. Lower panel: Histogram showing the distribution of $\Delta\log M_0$ residuals (GCMT minus RCMT seismic moment estimates) along with its mean and standard deviation (std). The vertical dashed line highlights the peaked zero difference.

as time passes and data from more stations are available for inversion. It should be also noted that before the year 2003 the GCMT group utilized only body waves in its inversions for moderate to small events. A clear outlier to this pattern is event 19970122, which occurred in southeast Turkey and also exhibits the largest residual of all 24 events. This event was large enough (*mb* = 5.5) to be recorded by many stations; however, it occurred in an area where the crustal thickness is much greater than the 25 km assumed by PREM. If this event is excluded, then the seismic moment residual of the rest correlate rather well with the number of stations used in each inversion.

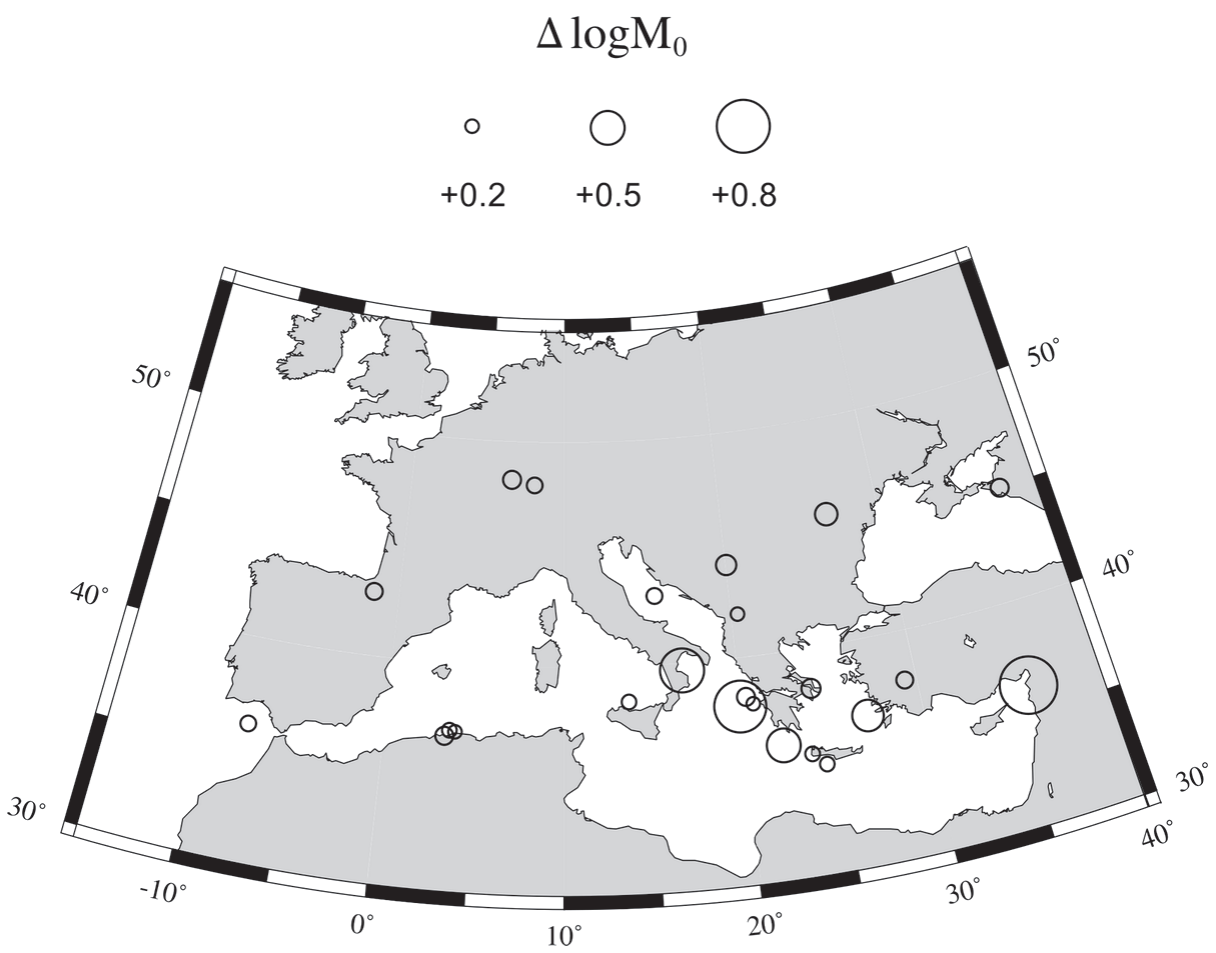

▲ **Figure 3.** Map of the EM region showing the geographical distribution of the 24 events that exhibit significant differences between GCMT and RCMT moment estimates (see also Table 1). The circle radius of each event is proportional to the moment residual $\Delta\log M_0$, whose scale is shown on top.

GCMT VERSUS SED SEISMIC MOMENTS

The final revised solutions of the SED catalog span the period 1999–2006; after that only automatic solutions are available. During this period 300 events were found with both a SED and GCMT moment tensor solution. A least-squares regression of the teleseismic and regional seismic moments shows that the regression line is very close to the 1:1 slope, and the linear correlation of the two is slightly higher than in the GCMT/RCMT case (Figure 6). The distribution of the seismic moment differences has a mean very close to zero, extending its tail toward the positive side but also exhibiting negative values that make it appear more symmetric. Here it is found that 57 events (19% of all the events) have either $\Delta\log M_0 > 0.20$ or have $\Delta\log M_0 < -0.20$, indicating overestimations and underestimations of more than 1.5 times between the GCMT and SED seismic moment. This time the geographical distribution of these events is not limited to the Mediterranean or mainland Europe, but rather extends across the Atlantic and the Middle East (Figure 7). Negative M_0 residuals are mostly located in the Atlantic and the Middle East, while the positive ones (which are also much larger in amplitude) appear in the Mediterranean, the Middle East, and the Caucasus area. Table 2 gives a summary of source parameters and other available information about these events. Again, it can be seen that the majority of the events exhibiting seismic moment differences are of shallow origin, with centroid depths less than 20 km.

The same set of factors (*mb*, crustal thickness, Kagan angles) that were examined previously are also investigated for the GCMT/SED dataset this time; however, we separate events based on their geographic location. Figure 8 shows the corresponding plots with different symbols for the three regions (Atlantic, Middle East, Europe) and for intermediate-depth events. Positive M_0 residuals mostly correspond to body wave magnitudes smaller than 5.0, while the negative ones span a wide range of magnitudes but the amplitude of the residual varies little. Three populations of events are seen as a function of crustal thickness: events occurring in the thin crust (< 10 km) of the Mid-Atlantic Ridge, events in the thick crust (>40 km) in the Caucasus and Middle East, and events in/around the Mediterranean where the crustal thickness is between 20 and 30 km. There does not seem to be a simple relationship between the residual sign and the crustal thickness of the source area, as one might expect from the synthetic tests of Hjörleifsdottir and

TABLE 1

Summary of source parameters for the 24 events that exhibit large GCMT-RCMT moment residuals. Epicentral locations are taken from the global relocation catalog of Engdahl *et al.* (1998) and its subsequent updates. OT is the origin time of each event. Three depth estimates are included, two of which (GCMT, RCMT) are centroid depths. *mb* is the body wave magnitude. θ is the Kagan angle and *h* (in km) is the crustal thickness at the source region of each event. Last two columns show the beachballs corresponding to the GCMT/RCMT moment tensor solutions.

				depth (km)								
Date	OT	Lat	Lon	PDE	GCMT	RCMT	*mb*	θ	*h*	$\Delta\log M_0$	GCMT	RCMT
19970122	17:57:24.95	36.199	35.902	10	15	16	5.3	20	43	0.85		
19990430	3:30:40.26	44.169	20.084	14	15	20	5.1	24	31	0.30		
20000421	12:23:11.9	37.85	29.353	33	15	18	4.8	43	35	0.26		
20000524	10:1:47.79	36.03	22.056	33	15	20	4.8	45	31	0.51		
20010720	5:9:41.22	45.76	26.649	127	134	129	4.9	66	41	0.34		
20011126	5:3:23.21	34.863	24.271	33	48	30	4.6	37	27	0.22		
20020417	6:42:57.21	39.687	16.925	5	15	15f	4.5	15	31	0.65		
20020728	17:16:31.42	37.94	20.76	22	22	22	4.8	30	27	0.21		
20020927	6:10:47.76	38.315	13.712	5	15	15f	4.4	15	20	0.21		
20021109	2:18:15.38	44.971	37.82	10	15	18	4.8	7	34	0.26		
20021209	9:35:7.83	37.839	20.044	10	15	15f	4.4	56	27	0.78		
20021210	13:51:32.14	36.267	–7.435	10	15	15f	4.3	32	32	0.23		
20030222	20:41:5.11	48.317	6.626	10	15	18	4.3	36	31	0.27		
20030522	3:14:4.97	36.96	3.645	10	15	15f	4.6	45	24	0.22		
20030522	13:57:23.29	36.971	3.917	10	15	15f	4.4	2	24	0.21		
20030529	2:15:1.96	36.817	3.301	10	15	15f	4.5	21	24	0.26		
20030913	13:46:15.81	36.658	26.885	155	160	163	5	31	31	0.47		
20031116	7:22:51.22	38.252	20.357	8	15	16	4.5	42	40	0.26		
20040724	19:0:56.7	35.313	23.574	11	12	15f	4.6	35	26	0.22		
20040918	12:52:17.48	42.869	–1.457	1	13	11f	4.8	72	36	0.24		
20040926	3:6:3.94	38.293	24.054	18	18	15f	4.3	29	30	0.29		
20041203	8:13:17.34	43.097	15.328	10	16	15f	4.2	35	16	0.24		
20041205	1:52:38.61	48.106	7.938	10	12	18	4.2	21	24	0.24		
20041209	18:35:20.12	41.991	20.421	4	28	15f	4.5	25	40	0.21		

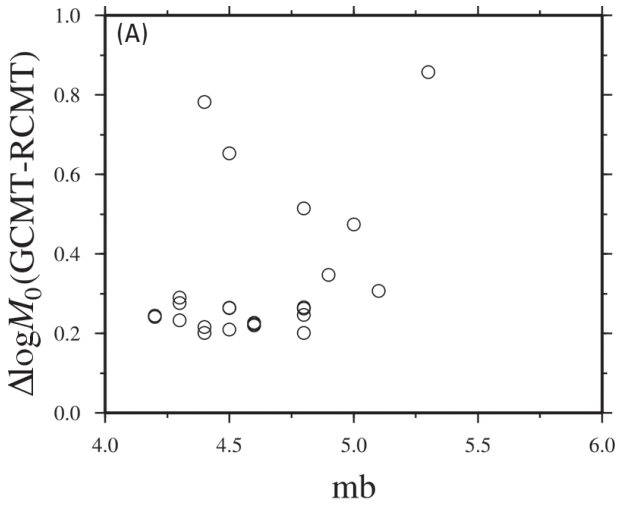

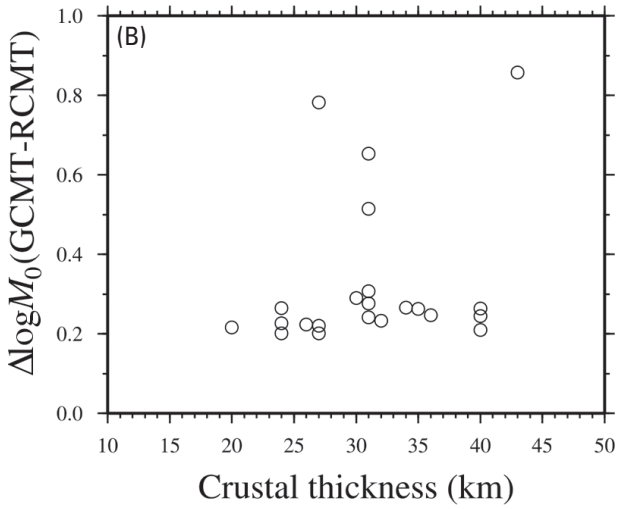

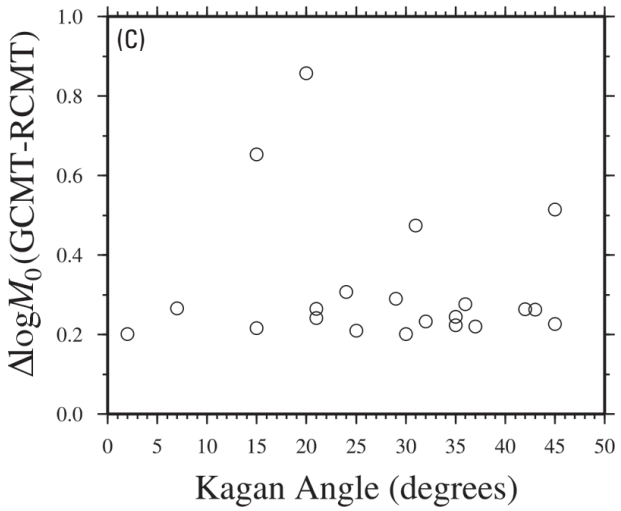

▲ **Figure 4.** Plot of GCMT-RCMT residual amplitude versus (A) body wave magnitude (*mb*), (B) crustal thickness at the source region of each event, and (C) the Kagan angle between GCMT and RCMT focal mechanism solutions.

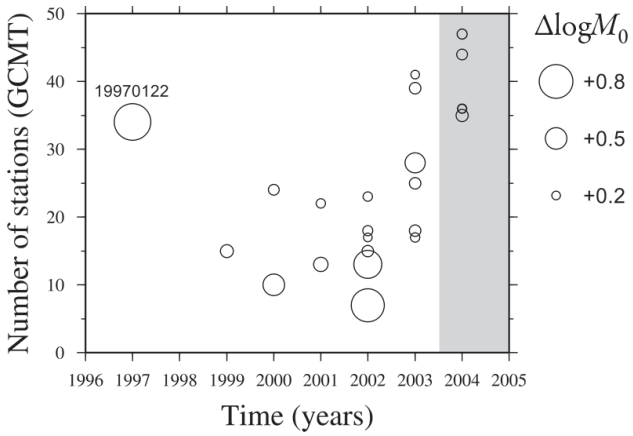

▲ **Figure 5.** Diagram showing the variation of GCMT-RCMT residual amplitude as a function of stations used in the GCMT inversion and as a function of time. The circle radius of each event is proportional to the moment residual $\Delta\log M_0$ whose scale is shown at the right-hand side. The gray shaded area represents the period when GCMT started inverting also surface waves for small to moderate events.

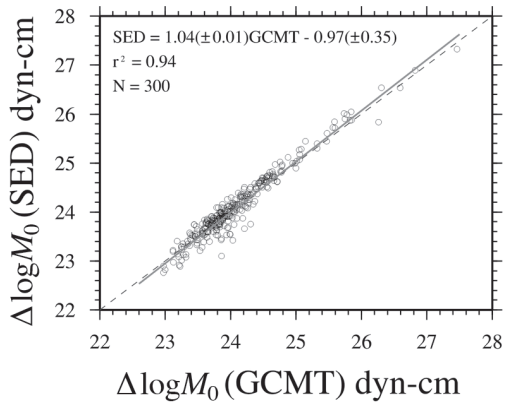

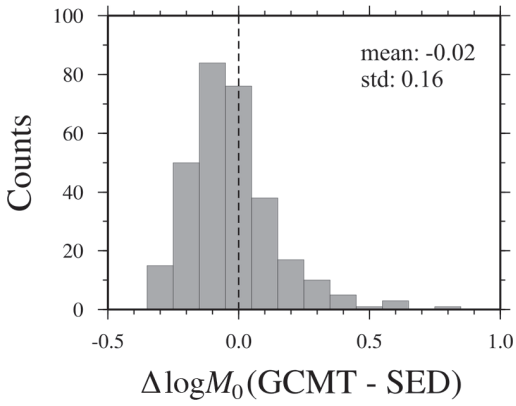

▲ **Figure 6.** Top panel: Linear regression results between RCMT and SED seismic moment estimates. All symbols are the same as in Figure 2. Lower panel: Histogram showing the distribution of $\Delta\log M_0$ residuals (GCMT minus SED seismic moment estimates) along with its mean and standard deviation (std). The vertical dashed line highlights the peaked zero difference.

TABLE 2
Summary of source parameters for the 57 events that exhibit large GCMT-SED moment residuals. All entries and symbols are the same as in Table 1.

				depth (km)								
Date	**OT**	**Lat**	**Lon**	**PDE**	**GCMT**	**SED**	***mb***	***θ***	***h***	**$\Delta\log M_0$**	**GCMT**	**SED**
20000220	10:42:41.47	56.026	−34.482	10	15	12	4.8	31	6.5	−0.30		
20000405	4:36:57.15	34.311	25.81	38	15	15	5.3	32	27	−0.21		
20000510	16:52:11.81	44.293	12.027	10	15	12	4.7	63	37	0.28		
20000524	10:1:47.79	36.03	22.056	33	15	24	4.8	52	31	0.42		
20000606	2:41:51.28	40.737	33.005	10	15	15	5.5	9	39	−0.21		
20000621	0:51:48.33	63.876	−20.748	10	15	27	6	17	11	−0.27		
20000621	14:56:27.8	70.737	−13.611	10	15	6	4.9	85	11	−0.30		
20000731	13:58:15.55	40.425	−29.445	10	15	15	5.1	4	6.57	−0.23		
20000821	17:14:29.36	44.835	8.453	10	15	4	4.6	34	31	−0.30		
20000823	13:41:29.94	40.778	30.772	15	15	30	5.1	47	32	−0.29		
20001125	18:9:13.18	40.198	49.929	50	15	33	5.7	47	44	0.42		
20001215	16:44:48.01	38.451	31.265	10	15	15	5.1	10	45	−0.21		
20010107	6:49:4.77	40.137	50.08	33	48	30	4.6	33	41	0.39		
20010328	16:34:22.41	29.925	51.276	33	15	15	4.7	41	41	0.30		
20010403	17:36:35.38	32.551	48.022	33	31	24	4.7	24	46	−0.28		
20010710	21:42:11.36	39.822	41.616	33	29	24	4.4	61	43	0.30		
20010720	5:9:41.22	45.76	26.649	128	134	129	4.9	63	41	0.27		
20010914	8:35:57.11	57.911	−32.509	10	15	12	5	38	6.57	−0.30		
20011126	5:3:23.21	34.863	24.271	33	48	42	4.6	59	27	0.27		
20020203	7:11:30.62	38.527	31.227	5	15	18	6.4	24	45	−0.21		
20020331	22:49:13.23	53.844	−35.369	10	15	12	5.2	28	6.5	−0.26		
20020417	6:42:57.21	39.687	16.925	5	15	12	4.5	37	31	0.61		
20020618	3:19:25.51	33.34	45.954	33	33	24	4.2	72	34	0.45		
20020622	2:58:23.21	35.597	49.02	10	15	18	6.4	20	46	−0.21		
20020916	18:48:27.71	66.917	−18.412	10	15	24	5.7	7	18.5	−0.27		
20020925	22:28:16.1	32.076	49.328	10	15	18	5.1	6	46	−0.22		
20021006	1:18:41.77	58.425	−31.787	10	15	12	5.3	25	10.6	−0.21		
20021109	2:18:15.38	44.971	37.82	10	15	33	4.8	30	34	0.55		

TABLE 2 (continued)
Summary of source parameters for the 57 events that exhibit large GCMT-SED moment residuals. All entries and symbols are the same as in Table 1.

				Depth (km)								
Date	**OT**	**Lat**	**Lon**	**PDE**	**GCMT**	**SED**	***mb***	***θ***	***h***	**$\Delta\log M_0$**	**GCMT**	**SED**
20021130	22:54:4.42	39.002	−28.435	10	15	9	4.7	71	10.6	−0.21		
20021209	9:35:7.83	37.839	20.044	10	15	63	4.4	97	27	0.76		
20021210	13:51:32.14	36.267	−7.435	10	15	9	4.3	27	32	0.27		
20030127	5:26:25.75	39.503	39.851	10	15	24	6	25	43	−0.30		
20030222	20:41:5.11	48.317	6.626	10	15	12	4.3	42	31	0.31		
20030501	0:27:6.93	38.97	40.458	10	15	21	6.3	12	43	−0.25		
20030521	18:44:21.5	36.88	3.694	12	15	18	6.8	20	24.5	−0.23		
20030527	10:30:51.12	29.491	51.264	33	33	33	4.2	54	41	0.43		
20030527	17:11:30.14	36.865	3.592	8	15	18	5.4	10	24.5	−0.21		
20030710	17:6:39.08	28.311	54.165	10	15	18	5.5	15	50	−0.28		
20030802	17:53:40.68	35.237	−35.848	10	15	9	4.6	15	6.57	0.22		
20030823	2:0:13.62	63.881	−22.218	10	15	12	4.4	8	11	0.24		
20030827	14:40:44.52	43.639	−28.87	10	15	12	4.9	23	6.57	−0.21		
20030830	1:4:44.01	73.195	6.533	10	15	6	4.7	42	7.5	0.55		
20030913	13:46:15.81	36.658	26.885	155	160	153	5	35	31	0.40		
20031024	5:58:23.34	28.309	54.049	33	33	15	4.4	27	50	−0.23		
20031121	4:9:12.05	45.226	−27.999	10	15	12	5.2	19	6.57	−0.26		
20040630	14:22:40.51	53.989	−35.174	10	12	9	4.8	16	6.57	−0.21		
20040917	14:8:7.59	58.666	−30.878	10	12	12	4.9	32	10.6	−0.29		
20041007	7:16:53.22	36.331	22.636	65	50	51	4.6	17	31	0.23		
20041202	3:30:4.6	36.979	−33.236	10	12	15	5	71	6.57	−0.27		
20041203	8:13:17.34	43.097	15.328	10	16	4	4.2	28	40	0.33		
20041205	1:52:38.61	48.106	7.938	10	12	12	4.2	20	31	0.29		
20041209	18:35:20.12	41.991	20.421	4	28	9	4.5	13	40	0.23		
20041213	14:16:11.05	36.225	−9.946	10	39	15	4.8	16	23	0.28		
20050111	4:36:1.08	36.92	27.851	35	15	12	5.1	12	31	−0.21		
20050125	11:39:20.44	33.374	45.878	45	12	24	4.9	27	34	−0.23		
20050125	16:44:16.06	37.603	43.691	41	13	24	5.3	19	34	−0.23		

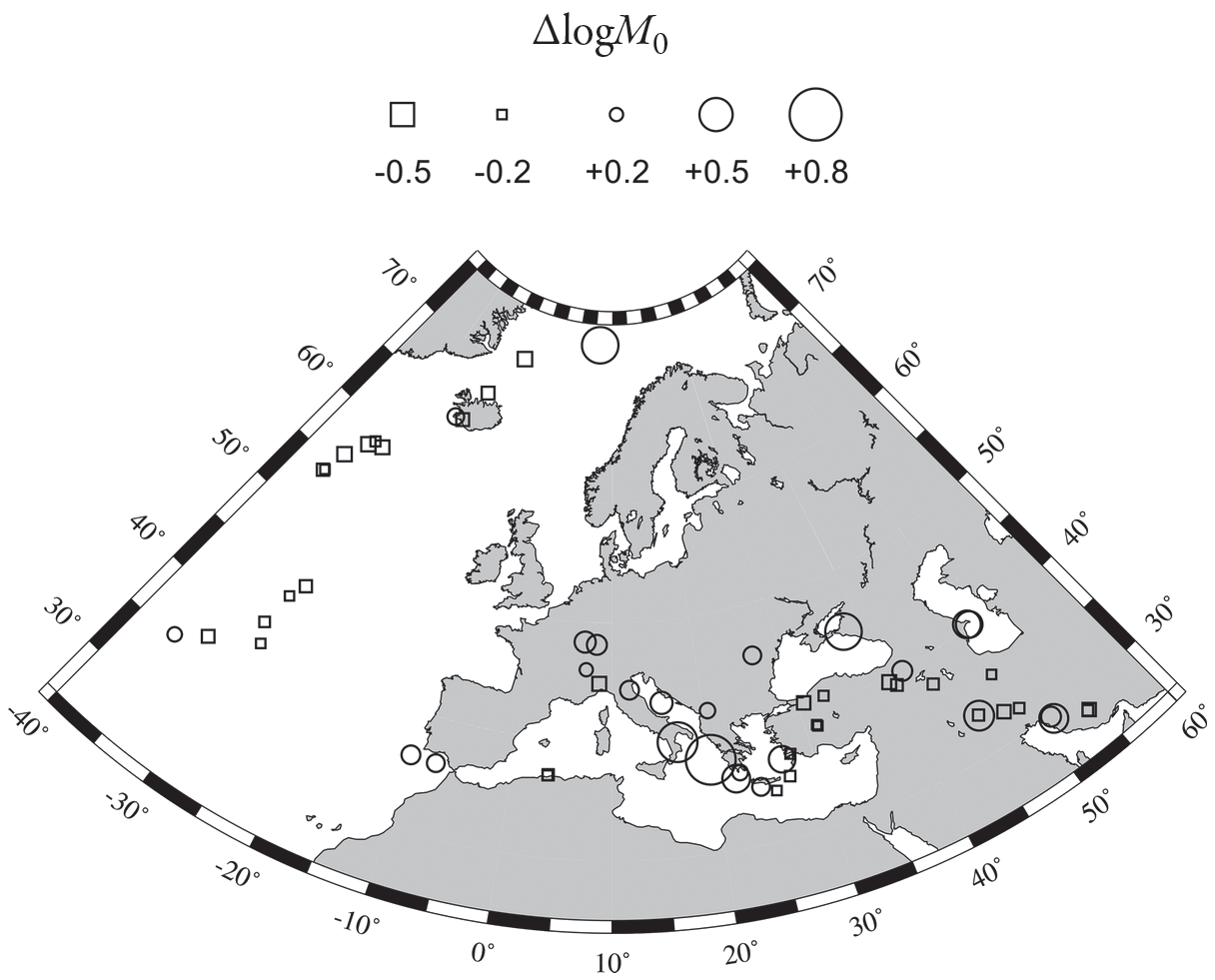

▲ **Figure 7.** Map of the broader EM region showing the geographical distribution of the 57 events that exhibit significant differences between GCMT and SED moment estimates (see also Table 2). Positive residuals are represented by circles and negative ones by squares. The circle radius/square size of each event is proportional to the moment residual $\Delta logM_0$, whose scale is shown on top.

Ekström (2010). On the other hand, the relationship between the residual amplitude and the Kagan angle is independent of geographic source location and exhibits a weak linear trend, which is more evident for the positive residuals. This implies that the amplitude of the residual is increasing when the GCMT and SED moment tensor solutions become more incompatible.

As in the case of the GCMT/RCMT catalog comparison, the small magnitude of the events with positive moment residuals points to the possibility that the number of stations may again be an influential factor. In order to investigate this a similar diagram to that shown in Figure 5 is created where the number of stations used in the GCMT inversions is shown as a function of time and residual amplitude for each event (Figure 9). In general, the largest residuals correlate with a small number (<20) of stations used in the GCMT inversion. There are, however, exceptions, such as event 20030830, which has a residual equal to 0.55 even though more than 30 stations were used for its moment tensor inversion. Residuals become smaller after the year 2003, as more stations are available and both body and surface waves are utilized in GCMT inversions in a similar fashion to the GCMT/RCMT case.

POSSIBLE CAUSES OF OBSERVED RESIDUALS

From the description given so far it is evident that the amplitude and distribution of seismic moment residuals depend on which regional catalog (RCMT, SED) is used for comparison with GCMT. In the case of GCMT versus RCMT seismic moments, all residuals have a positive sign indicating a potential overestimation of the teleseismic M_0 value. However, the amplitude of the residual shows no simple relationship with any of the examined parameters that could influence seismic moment differences (*mb*, crustal thickness, Kagan angle). On the other hand, an increasing number of stations used in the GCMT inversions seems to be an important factor that can reduce the residual amplitude. The usage of more than one wave type, except from body waves, also has an influence on reducing the residuals, confirming the synthetic tests of Hjörleifsdottir and Ekström (2010). Crustal thickness seems to play an important role in seismic moment overestimation when it approaches values of over 40 km, as attested by the only event with a large residual that occurred in 43-km thick crust.

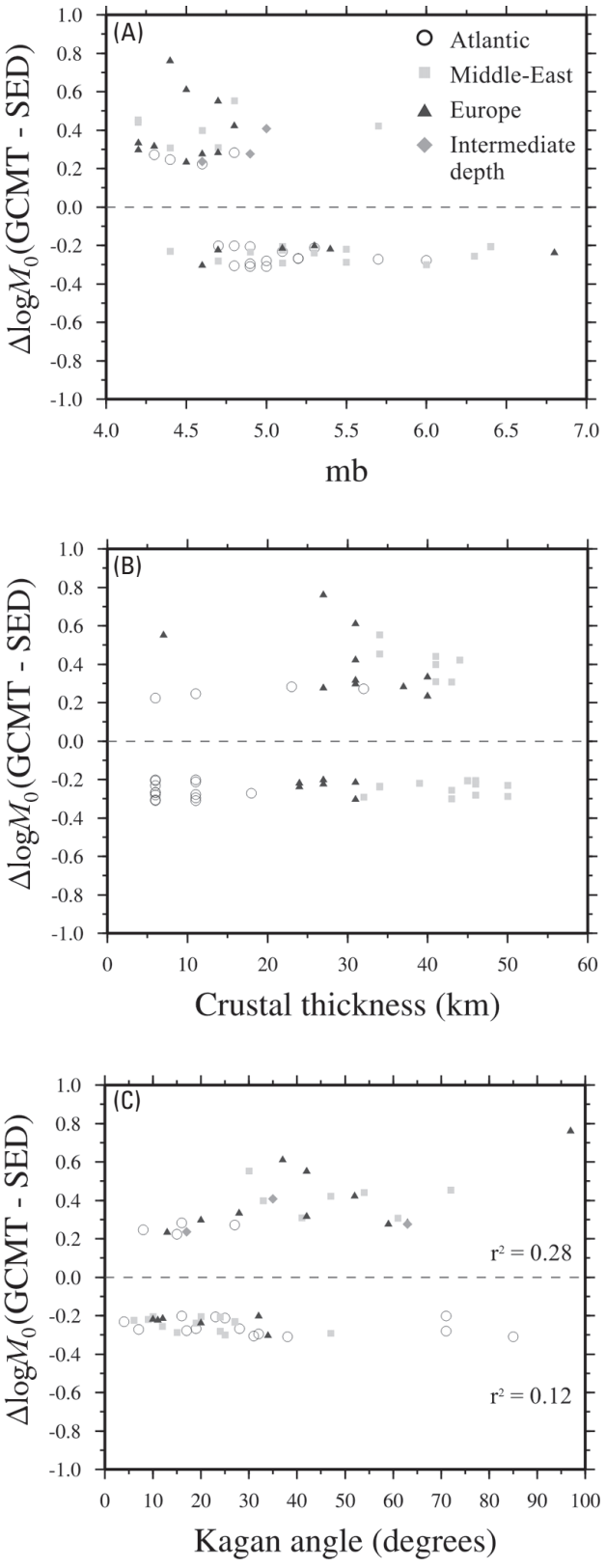

▲ **Figure 8.** Plot of GCMT-SED residual amplitude versus (A) body wave magnitude (*mb*), (B) crustal thickness at the source region of each event, and (C) the Kagan angle between GCMT and SED focal mechanism solutions. Plotted symbols follow the grouping shown at the top right of (A).

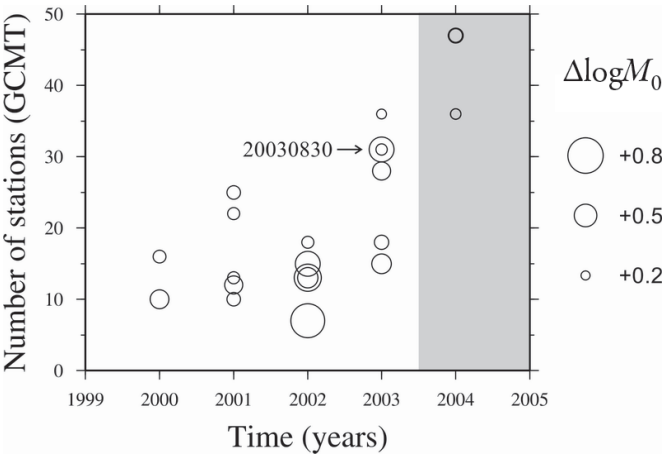

▲ **Figure 9.** Diagram showing the variation of GCMT-SED residual amplitude as a function of stations used in the GCMT inversion and as a function of time. The circle radius of each event is proportional to the moment residual $\Delta logM_0$, whose scale is shown at the right-hand side. The gray shaded area represents the period when GCMT started inverting also surface waves for small to moderate events.

The GCMT-SED residuals display different characteristics from their GCMT-RCMT counterparts, and these characteristics seem to depend at least partly on the source location of the events. Almost all earthquakes along the Mid-Atlantic Ridge have negative residuals, which means that the teleseismic moment estimate is smaller. This observation is apparently in agreement with the results of Hjörleifsdottir and Ekström (2010), where the thin oceanic crust has been found to cause such an underestimation. It should be noted that most events have occurred before 2003 and therefore only body waves were used to derive their GCMT solutions.

The residual observations for events occurring in eastern Turkey and the Middle East are more interesting, from the point of view that most of these events are large ($mb > 5.6$) and one would not expect significant differences in seismic moment estimates. Even though many of them originated in thick crust (40 km or more), they exhibit positive but also negative residuals. A closer look at the events that have negative residuals (smaller SED seismic moment) reveals that the corresponding GCMT inversion used more than one wave type, so it is expected that the teleseismic moment is probably well-constrained. The SED database provides waveform inversion fits and the azimuth/epicentral distance of each station used in the inversion. From this information it can be seen that in most cases the closest stations available for these events had an epicentral distance of 800 km or more. The waveforms of these stations are clearly dominated by high-amplitude surface waves while body waves represent only a minor part at the beginning of the signal. Since the events are located far away from mainland Europe, the PREM velocity model is used for Green's function calculations. Ferreira and Woodhouse (2006) have shown that inversion of surface waves using one-dimensional velocity models without corrections for lateral heterogeneity may result in large values for $M_{r\varphi}$ and $M_{r\vartheta}$ (corresponding to $-M_{yz}$ and M_{xz} in

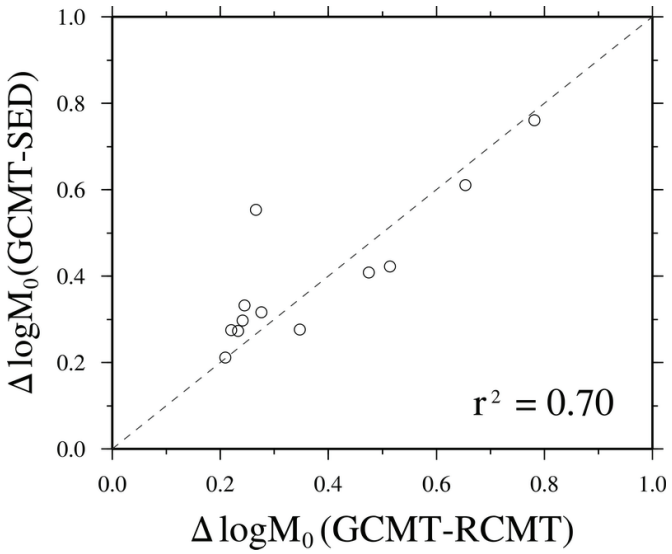

▲ **Figure 10.** Diagram showing the comparison of GCMT-SED and GCMT-RCMT residuals for 12 common events that occurred around the Mediterranean. The two quantities exhibit linear correlation and confirm a consistent overestimation of the teleseismic moment estimate.

the co-ordinate system used by SED) moment tensor elements. This can result in biasing seismic moment estimates, a problem particularly acute for shallow earthquakes like the ones dealt with here. On the other hand, events that have a larger teleseismic moment are smaller (mb < 5), and GCMT solutions have been derived using only body waves, so it is possible that M_0 is overestimated due to the large crustal thickness (the same applies for the events around the Caucasus/Caspian Sea).

Most earthquakes in the Mediterranean and mainland Europe exhibit small body wave magnitudes while the sign of the residual is mixed. The majority have larger teleseismic moments, even though the crustal thickness in the region is close to the value assumed by PREM. For 12 events in this area both GCMT-RCMT and GCMT-SED residuals are available. Their comparison shows that they are linearly correlated, which means that teleseismic moments for these 12 events are consistently overestimated (Figure 10). The most likely reason for this, as stated before, is the limited number of available stations and the use of only one wave type during GCMT inversions. Event 20030521 occurred offshore of the coast of northern Algeria and is one of the few events with negative residuals and the largest event of this group (mb ~6.8). As might be expected the GCMT solution has been derived using all available wave types (body, surface, mantle); therefore this may be a case of SED moment overestimation. The cause of this overestimation may again lie in the shallow origin of the event (centroid depth 15–18 km), which results in poorly constrained moment tensor elements as mentioned before. It should be noted that there are a small number of events with large residuals that do not seem to be caused by any of the reasons presented previously. One such example is event 20030830, which occurred offshore Greenland and has a large positive residual (see Figure 7 and Table 2)—it has, however, originated in thin crust and many stations were available in the GCMT inversion. The cause of these enigmatic residuals can only be revealed through additional waveform modeling and by testing different algorithms, station configurations, and velocity models.

Finally, there is an open question whether these differences in teleseismic and regional moment estimates remain consistent if teleseismic moments determined by the U.S. Geological Survey are used instead of those by GCMT. In the case of the RCMT estimates only one event (19970122) has a corresponding USGS solution and its residual amplitude (~0.87) is similar to that of GCMT-RCMT (~0.85). For the events reported by SED, 17 of them have a USGS solution and their characteristics are summarized in Table 3 in the same way as in the other tables. It can be seen that with the exception of four events (20000606, 20001125, 20030527, 20030827), all the others show similar or even larger negative residuals between the teleseismic and regional moment estimates. Once more, consistency between the two moment tensor solutions does not imply consistency in seismic moments (see, for example, event 20030127).

CONCLUSIONS

The main conclusions of this study can be summarized as follows:

1. Both catalog comparisons (GCMT/RCMT, GCMT/SED) in the EM region show a similar amount (19%–20%) of events that exhibit differences of more than 1.5 times between the teleseismic and regional seismic moment estimates. The majority of these events have a shallow origin (<20 km) and occur at different tectonic settings. In the case of GCMT/RCMT the residuals are found always to be positive while for GCMT/SED the residuals can be either positive or negative.
2. Positive residuals (teleseismic moment is larger) can be correlated with large crustal thickness (>40 km) in the source region, limited number of available stations, and inclusion of only one type of waves (usually body waves) in the GCMT inversion.
3. Negative residuals (regional moment is larger) are the result of either GCMT moment underestimation caused by small crustal thickness (<10 km) in the source region or the inability to obtain a well-constrained moment tensor by inverting regional waveforms that are dominated by surface waves in the case of a shallow source.
4. These observations agree in general with previous studies on this subject in central Asia (Patton 1998; Patton and Randall 2002) and with the most recent simulation tests for GCMT inversions (Ferreira and Woodhouse 2006; Hjörleifsdottir and Ekström 2010). It also seems that similar results can be obtained if USGS moments are used in the comparisons instead of those of GCMT. Future efforts should focus on waveform modeling while using the same algorithms and data that the different groups have employed in order to infer the relative contribution of possible causes for the residuals reported here.

TABLE 3
Summary of source parameters for the 17 events that have USGS-SED residuals. All entries and symbols are the same as in Table 1.

Date	OT	Lat	Lon	Depth (km) USGS	Depth (km) SED	*mb*	*θ*	*h*	$\Delta\log M_0$ (GCMT-SED)	$\Delta\log M_0$ (USGS-SED)	USGS	SED
20000606	2:41:51.28	40.737	33.005	3	15	5.5	28	39	−0.21	−0.15		
20000621	00:51:48.33	63.876	−20.748	14	27	6	27	11	−0.27	−0.31		
20001125	18:09:13.18	40.198	49.929	35	33	5.7	18	44	0.42	−0.43		
20001215	16:44:48.01	38.451	31.265	7	15	5.1	23	45	−0.21	−0.32		
20020203	7:11:30.62	38.527	31.227	22	18	6.4	66	45	−0.21	−0.61		
20020622	2:58:23.21	35.597	49.02	5	18	6.4	5	46	−0.21	−0.21		
20020916	18:48:27.71	66.917	−18.412	20	24	5.7	48	18.5	−0.27	−0.28		
20020925	22:28:16.10	32.076	49.328	7	18	5.1	7	46	−0.22	−0.36		
20021006	1:18:41.77	58.425	−31.787	4	12	5.3	33	10.6	−0.21	−0.20		
20030127	5:26:25.75	39.503	39.851	9	24	6	28	43	−0.30	−0.40		
20030501	00:27:06.93	38.97	40.458	15	21	6.3	14	43	−0.25	−0.23		
20030521	18:44:21.50	36.88	3.694	9	18	6.8	25	24.5	−0.23	−0.43		
20030527	17:11:30.14	36.865	3.592	4	18	5.4	13	24.5	−0.21	−0.08		
20030710	17:06:39.08	28.311	54.165	24	18	5.5	105	50	−0.28	−0.57		
20030827	14:40:44.52	43.639	−28.87	3	12	4.9	10	6.57	−0.21	0.03		
20031121	4:09:12.05	45.226	−27.999	4	12	5.2	26	6.57	−0.26	−0.26		
20050125	16:44:16.06	37.603	43.691	14	24	5.3	71	34	−0.23	−0.36		

ACKNOWLEDGMENTS

We would like to thank the National Science Council of Taiwan for financial support of this study in the form of a research grant awarded to K. I. Konstantinou and a postdoctoral fellowship to S. Rontogianni. Thanks are also due to Jonathan M. Lees for the editorial handling of the manuscript and Silvia Pondrelli for her helpful suggestions.

REFERENCES

Aki, K. (1966). Generation and propagation of *G* waves from the Niigata earthquake of June 16, 1964. 2. Estimation of earthquake movement, released energy, and stress-strain drop from *G* wave spectrum. *Bulletin of the Earthquake Institute, University of Tokyo* **44**, 23–88.

Arvidsson, R., and G. Ekström (1998). Global CMT analysis of moderate earthquakes, *Mw* > 4.5, using intermediate-period surface waves. *Bulletin of the Seismological Society of America* **88**, 1,003–1,013.

Bassin, C., G. Laske, and G. Masters (2000). The current limits of resolution for surface wave tomography in North America. *Eos, Transactions, American Geophysical Union* **81** (F897). Also available at http://igppweb.ucsd.edu/~gabi/crust2.html

Braunmiller, J., U. Kradolfer, M. Baer, and D. Giardini (2002). Regional moment tensor determination in the European-Mediterranean area—initial results. *Tectonophysics* **356**, 5–22.

Dziewonski, A. M., and D. L. Anderson (1981). Preliminary reference Earth model. *Physics of the Earth and Planetary Interiors* **25**, 297–356.

Dziewonski, A. M., T. A. Chou, and J. H. Woodhouse (1981). Determination of earthquake source parameters from waveform data for studies of global and regional seismicity. *Journal of Geophysical Research* **86**, 2,825–2,852.

Dziewonski, A. M., G. Ekström, and M. P. Salganik (1992). Centroid-moment tensor solutions for July–September 1991. *Physics of the Earth and Planetary Interiors* **72**, 1–11.

Ekström, G., J. Tromp, and E. W. F. Larson (1997). Measurements and global models of surface wave propagation. *Journal of Geophysical Research* **102**, 8,137–8,157.

Engdahl, E. R., R. D. van der Hilst, and R. P. Buland (1998). Global teleseismic earthquake relocation with improved travel time and procedures for depth determination. *Bulletin of the Seismological Society of America* **88**, 722–743.

Ferreira, A. M. G., and J. H. Woodhouse (2006). Long-period seismic source inversions using global tomographic models. *Geophysical Journal International* **166**, 1,178–1,192; doi:10.1111/j.1365-246X.2006.03003.x.

Hjörleifsdottir, V., and G. Ekström (2010). Effects of three-dimensional Earth structure on CMT earthquake parameters. *Physics of the Earth and Planetary Interiors* **179**, 178–190; doi:10.1016/j.pepi.2009.11.003.

Kagan, Y. Y. (1991). 3-D rotation of double-couple earthquake sources. *Geophysical Journal International* **106**, 709–716.

Nabelek, J., and G. Xia (1995). Moment tensor analysis using regional data: Application to the 25 March 1993, Scotts Mills, Oregon, earthquake. *Geophysical Research Letters* **22**, 13–16.

Patton, H. J. (1998). Bias in the centroid moment tensor for central Asian earthquakes: Evidence from regional surface wave data. *Journal of Geophysical Research* **103**, 26,963–26,974.

Patton, H. J., and G. E. Randall (2002). On the causes of biased estimates of seismic moment for earthquakes in central Asia. *Journal of Geophysical Research* **107**, 2,302; doi:10.1029/2001JB000351.

Pondrelli, S., A. Morelli, and G. Ekström (2004). European-Mediterranean regional centroid-moment tensor catalog: Solutions for years 2001 and 2002. *Physics of the Earth and Planetary Interiors* **145**, 127–147; doi:10.1016/j.pepi.2004.03.008.

Pondrelli, S., A. Morelli, G. Ekström, S. Mazza, E. Boschi, and A. M. Dziewonski (2002). European-Mediterranean centroid-moment tensors: 1997–2000. *Physics of the Earth and Planetary Interiors* **130**, 71–101.

Pondrelli, S., A. Morelli, and G. Ekström, 2004. European-Mediterranean regional centroid-moment tensor catalog: solutions for years 2001 and 2002. *Physics of the Earth and Planetary Interiors* **145**, 127–147, doi:10.1016/j.pepi.2004.03.008.

Priestley, K. F., and H. J. Patton (1997). Calibration of *mb*(*Pn*), *mb*(*Lg*) scales and transportability of the M_0:*mb* discriminant to new tectonic regions. *Bulletin of the Seismological Society of America* **87**, 1,083–1,099.

Institute of Geophysics
National Central University
Jhongli, 320 Taiwan
kkonst@ncu.edu.tw
(K. I. K.)